Axisymmetric vesicles under point force loading

Kumar Gaurav

Roll number: 20105271
gmail id: kumgaurav5620@gmail.com
IIT Kanpur

Tuesday 22nd November, 2022

Number of hours spent in papers/books collection	5 hrs.
Number of hours spent in reading and understanding the relevant papers/books/topics	hrs.
Number of hours spent in typing the report	hrs.
Number of hours spent in proof-reading your report before final submission and making it error free	hrs.

1 Introduction

External forces when applied on a vesicle can result in the formation of microtubes also known as tethers. This formation of tether can be studied as deformation of vesicles under axial loading. The deformed shape under the axial loading depends on the elastic properties of the membrane and hence the theoretical results can be compared with the experimental observations to obtain elastic properties of the membrane. Because of the small radius, the effects of the bending is significant in the tethers and can be used to estimate both local and non-local membrane bending modulus.

In this report, I will discuss the shape change due to application of equal and opposite point forces on a vesicle with known equilibrium shapes. The nature of forces can be both pushing or pulling. Owing to the fluid nature of its membrane, initially the vesicle only changes its orientation such that the point forces acts along the largest possible distance possible for any two points of the membrane. This reorientation doesn't cost any energy. For a prolate spheroid,the forces will act along its poles and hence the symmetry of the shape is not broken. However, for an oblate spheroid, the forces acts along the longer axis (on the equator) and hence the symmetry is broken.

2 Shape equations for the axially strained vesicles

The elastic energy of the membrane using Area Difference Elasticity (ADE) can be written as

$$E = W_{RE} + W_b \tag{1}$$

where W_{RE} is the relative expansivity term and W_b is the bending energy term. The area expansivity term is written as

$$W_{RE} = \frac{k_r}{2Ah^2}(\Delta A - \Delta A_0)^2, \tag{2}$$

where k_r is the non-local bending modulus, ΔA and ΔA_0 are the differences between the areas of the outer and the inner monolayers at the deformed and reference state, respectively. Furthermore,

$$\Delta A = h \int (c_1 + c_2) dA, \tag{3}$$

where c_1 and c_2 are the principal curvatures and h is the distance between the monolayers. The bending energy is expressed as

$$W_b = \frac{1}{2} k_c \int (c_1 + c_2)^2 dA, \tag{4}$$

where k_c is the bending modulus.The spontaneous curvature c_0 is taken to be zero because we are taking a symmetrical bilayer membrane and also the Gaussian bending term is ignored because it is constant for a given topology. The energy functional of an axially strained vesicle can be written as

$$G = W_{RE} + W_b - \mu V - \lambda A - f Z_0, \tag{5}$$

where μ and λ are Lagrange multiplier for volume and area constraints and f is the Lagrange multiplier corresponding to the distance between the poles Z_0. The above Lagrangian can be non-dimensionalized using a length scale R_0 such that the area of the sphere with the radius R_0 is equal to the area of the vesicle. In other words $R_0 = \sqrt{A/4\pi}$. The non-dimensionalized quantities are

$$a = \frac{A}{4\pi R_0^2}, \qquad v = \frac{V}{\frac{4\pi R_0^3}{3}}, \qquad \Delta a = \frac{\Delta A}{4\pi (R_0 + h)^2 - 4\pi (R_0)^2} = \frac{\Delta A}{8\pi h R_0}, \qquad \Delta a_0 = \frac{\Delta A_0}{8\pi h R_0}$$
$$z_0 = \frac{Z_0}{R_0}, \qquad w_b = \frac{W_b}{\frac{k_c}{2} \int \left(\frac{2}{R}\right)^2 dA} = \frac{W_b}{8\pi k_c}, \qquad w_{RE} = \frac{W_{RE}}{8\pi k_c} = \frac{k_r}{k_c} (\Delta a - \Delta a_0)^2, \qquad \text{and} \qquad g = \frac{G}{8\pi k_c}. \tag{6}$$

Using (6) in (5), we obtain the non-dimensionalized form of the energy functional

$$g = w_{RE} + w_b - M v - L a - F z_0, \tag{7}$$

where

$$M = \frac{R_0^3}{6 k_c} \mu, \qquad L = \frac{R_0^2}{2 k_c} \lambda \qquad \text{and} \qquad F = \frac{R_0}{8\pi k_c} f \tag{8}$$

are non-dimensionalized Lagrange multipliers.

The axisymmetric surface is shown in Fig. 1. $r(s)$ is the distance from the symmetry axis, s is the arc length, $z(s)$ is the distance along the symmetry axis and $\psi(s)$ is the angle of the contour. From the Fig. 1, we have the following relations

$$\begin{aligned}
\frac{dr(s)}{ds} &= \cos\psi(s), \\
\frac{dz(s)}{ds} &= \sin\psi(s), \\
da &= \frac{dA}{4\pi R_0^2} = \frac{2\pi r(s) ds}{4\pi R_0^2} = \frac{\hat{r}(\hat{s}) d\hat{s}}{2} \\
dv &= \frac{dV}{\frac{4\pi R_0^3}{3}} = \frac{\pi r^2(s) dz}{\frac{4\pi R_0^3}{3}} = \frac{3}{4} \hat{r}^2(\hat{s}) \sin\psi(\hat{s}) d\hat{s},
\end{aligned} \tag{9}$$

where $\hat{r}$ and $\hat{s}$ are non-dimensionalized value of r and s, respectively. The mean curvature for the axisymmetric vesicles has been derived in project 2 equation 12 [2]. Using the above relations and expressions for the mean

curvature, the energy functional (7) becomes

$$g = \frac{1}{16\pi k_c} k_c \oint (2H(s))^2 dA + \frac{k_r}{k_c}(\Delta a - \Delta a_0)^2 - L \oint da - M \oint dv - F \oint dz$$
$$= \int_{\hat{s}_0}^{\hat{s}_1} \frac{\hat{r}(\hat{s})}{8} \left(\frac{d\psi(\hat{s})}{d\hat{s}} + \frac{\sin\psi(\hat{s})}{r(\hat{s})} \right)^2 d\hat{s} + \frac{k_r}{k_c}(\Delta a - \Delta a_0)^2 - L \int_{\hat{s}_0}^{\hat{s}_1} \hat{r}(\hat{s}) d\hat{s} - M \int_{\hat{s}_0}^{\hat{s}_1} \frac{3\hat{r}^2(s)\sin\psi(\hat{s})}{4} d\hat{s} - F \int_{\hat{s}_0}^{\hat{s}_1} \sin\psi(\hat{s}) d\hat{s}$$

The contour angle $\psi(\hat{s})$ and distance $r(\hat{s})$ are related by the relation given in (9). Therefore, the minimization problem will contain an extra term

$$g = \int_{\hat{s}_0}^{\hat{s}_1} \frac{\hat{r}(\hat{s})}{8} \left(\frac{d\psi(\hat{s})}{d\hat{s}} + \frac{\sin\psi(\hat{s})}{r(\hat{s})} \right)^2 d\hat{s} + \frac{k_r}{k_c}(\Delta a - \Delta a_0)^2 - L \int_{\hat{s}_0}^{\hat{s}_1} \hat{r}(\hat{s}) d\hat{s} - M \int_{\hat{s}_0}^{\hat{s}_1} \frac{3\hat{r}^2(s)\sin\psi(\hat{s})}{4} d\hat{s}$$
$$- F \int_{\hat{s}_0}^{\hat{s}_1} \sin\psi(\hat{s}) d\hat{s} + \int_{\hat{s}_0}^{\hat{s}_1} \Gamma(\hat{s}) \left(\frac{d\hat{r}(\hat{s})}{d\hat{s}} - \cos\psi(\hat{s}) \right) d\hat{s}$$

Finding minima of g w.r.t Δa gives the equilibrium condition

$$\left.\frac{\partial g}{\partial \Delta a}\right|_{eq} = \left.\frac{\partial (w_b + w_{RE})}{\partial \Delta a}\right|_{eq}$$
$$\implies \left.\frac{\partial w_b}{\partial \Delta a}\right|_{eq} = -\left.\frac{\partial w_{RE}}{\partial \Delta a}\right|_{eq} = -2\frac{k_r}{k_c}(\Delta a - \Delta a_0) = N \tag{10}$$

The variation of the relative expansivity term can be written as

$$\delta w_{RE} = \delta(\Delta a) \left.\frac{dw_{RE}}{d\Delta a}\right|_{eq} = -N\delta(\Delta a) = -N\delta \int_{\hat{s}_0}^{\hat{s}_1} \frac{\hat{r}(\hat{s})}{4} \left(\frac{d\psi(\hat{s})}{d\hat{s}} + \frac{\sin\psi(\hat{s})}{r(\hat{s})} \right) d\hat{s} \tag{11}$$

The variation of the energy functional become

$$\delta g = \delta \int_{\hat{s}_0}^{\hat{s}_1} \frac{\hat{r}(\hat{s})}{8} \left(\frac{d\psi(\hat{s})}{d\hat{s}} + \frac{\sin\psi(\hat{s})}{r(\hat{s})} \right)^2 d\hat{s} + \delta\frac{k_r}{k_c}(\Delta a - \Delta a_0)^2 - L\delta \int_{\hat{s}_0}^{\hat{s}_1} \frac{\hat{r}(\hat{s})}{2} d\hat{s} - M\delta \int_{\hat{s}_0}^{\hat{s}_1} \frac{3\hat{r}^2(s)\sin\psi(\hat{s})}{4} d\hat{s}$$
$$- F\delta \int_{\hat{s}_0}^{\hat{s}_1} \sin\psi(\hat{s}) d\hat{s} + \delta \int_{\hat{s}_0}^{\hat{s}_1} \Gamma(\hat{s}) \left(\frac{d\hat{r}(\hat{s})}{d\hat{s}} - \cos\psi(\hat{s}) \right) d\hat{s}$$
$$= \delta \int_{\hat{s}_0}^{\hat{s}_1} \left\{ \frac{\hat{r}(\hat{s})}{8} \left(\frac{d\psi(\hat{s})}{d\hat{s}} + \frac{\sin\psi(\hat{s})}{r(\hat{s})} \right)^2 - \frac{N}{4} \left(\frac{d\psi(\hat{s})}{d\hat{s}} \hat{r}(\hat{s}) + \sin\psi(\hat{s}) \right) - L\frac{\hat{r}(\hat{s})}{2} - M\frac{3\hat{r}^2(s)\sin\psi(\hat{s})}{4} \right.$$
$$\left. - F\sin\psi(\hat{s}) + \Gamma(\hat{s}) \left(\frac{d\hat{r}(\hat{s})}{d\hat{s}} - \cos\psi(\hat{s}) \right) \right\} d\hat{s}$$
$$= \delta \int_{\hat{s}_0}^{\hat{s}_1} \mathcal{L} d\hat{s}, \tag{12}$$

The minima is achieved where the first variation is zero. Let us consider the variation of the form

$$\begin{aligned} \psi_\varepsilon(s) &= \psi(s) + \epsilon\alpha(s), \\ r_\varepsilon(s) &= \rho(s) + \epsilon\beta(s), \\ s_{0\varepsilon} &= s_0 + \varepsilon\zeta_0, \qquad \psi_{0\varepsilon} = \psi_0 + \varepsilon\eta_0, \qquad r_{0\varepsilon} = r_0 + \varepsilon\gamma_0 \\ s_{1\varepsilon} &= s_1 + \varepsilon\zeta_1, \qquad \psi_{1\varepsilon} = \psi_1 + \varepsilon\eta_1, \qquad r_{1\varepsilon} = r_1 + \varepsilon\gamma_1, \end{aligned} \tag{13}$$

where $\psi_0 = \psi(s_0)$, $r_0 = r(s_0)$, $\psi_1 = \psi(s_1)$ and $r_1 = r(s_1)$.We have removed ˆ for the simplicity of notation and will continue to do so in further equations. Also at the end points these variations satisfy following relations

$$\begin{aligned} \dot{\psi}(s_0)\zeta_0 + \alpha(s_0) &= \eta(s_0), \qquad \dot{r}(s_0)\zeta_0 + \beta(s_0) = \gamma(s_0) \\ \dot{\psi}(s_1)\zeta_1 + \alpha(s_1) &= \eta(s_1), \qquad \dot{r}(s_1)\zeta_1 + \beta(s_1) = \gamma(s_1) \end{aligned} \tag{14}$$

where $(\dot{})$ represents derivative w.r.t s. Calculating the first variation of the functional g,

$$\frac{d}{d\varepsilon} g\left(\psi_\varepsilon, \dot{\psi}_\varepsilon, r_\varepsilon, \dot{r}_\varepsilon,\right)\Big|_{\varepsilon=0} = \frac{d}{d\varepsilon}\int_{s_0}^{s_1} \mathcal{L}\left(r_\varepsilon, \dot{r}_\varepsilon, \psi_\varepsilon, \dot{\psi}_\varepsilon,\right) ds\Big|_{\varepsilon=0},$$

Upon using the Taylor's series expansion and integral by parts (described in Project 2 [2]), the above expansion becomes

$$\begin{aligned}\frac{d}{d\varepsilon} g\left(\psi_\varepsilon, \dot{\psi}_\varepsilon, r_\varepsilon, \dot{r}_\varepsilon\right)\Big|_{\varepsilon=0} &= \int_{s_0}^{s_1}\left[\left\{\frac{\partial\mathcal{L}}{\partial\psi} - \frac{d}{ds}\left(\frac{\partial\mathcal{L}}{\partial\dot{\psi}}\right)\right\}\alpha(s) + \left\{\frac{\partial\mathcal{L}}{\partial r} - \frac{d}{ds}\left(\frac{\partial\mathcal{L}}{\partial\dot{r}}\right)\right\}\beta(s)\right] ds \\ &+ \left[\frac{\partial\mathcal{L}}{\partial\dot{\psi}}\alpha(s)\right]_{s_0}^{s_1} + \left[\frac{\partial\mathcal{L}}{\partial\dot{r}}\beta(s)\right]_{s_0}^{s_1} + \left[\zeta_1\mathcal{L}\Big|_{s_1} - \zeta_0\mathcal{L}\Big|_{s_0}\right].\end{aligned}$$

Making the first variation go to zero and since $\alpha(s)$ and $\beta(s)$ are independent variations, gives the following equations

$$\begin{aligned}\frac{\partial\mathcal{L}}{\partial\psi} - \frac{d}{ds}\left(\frac{\partial\mathcal{L}}{\partial\dot{\psi}}\right) &= 0, \\ \frac{\partial\mathcal{L}}{\partial r} - \frac{d}{ds}\left(\frac{\partial\mathcal{L}}{\partial\dot{r}}\right) &= 0,\end{aligned} \tag{15}$$

The boundary conditions upon using the relation (14) gives

$$\begin{aligned}\left[\frac{\partial\mathcal{L}}{\partial\dot{\psi}}\eta\right]_{s_0}^{s_1} &= 0 \\ \left[\frac{\partial\mathcal{L}}{\partial\dot{r}}\gamma\right]_{s_0}^{s_1} &= 0 \\ \left[\left(\mathcal{L} - \frac{\partial L}{\partial\dot{\psi}}\dot{\psi} - \frac{\partial L}{\partial\dot{r}}\dot{r}\right)\zeta\right]_{s_0}^{s_1} &= [H\zeta]_{s_0}^{s_1} = 0,\end{aligned} \tag{16}$$

where H is the Hamiltonian of the functional g. Since $\mathcal{L}$ doesn't depend explicitly on the arc length parameter, H remains constant on the curve. Also, ζ_1 and ζ_2 are arbitrary and hence from the boundary conditions (16), we get an extra condition

$$H = \mathcal{L} - \frac{\partial\mathcal{L}}{\partial\dot{\psi}}\dot{\psi} - \frac{\partial\mathcal{L}}{\partial\dot{r}}\dot{r} = 0. \tag{17}$$

To derive the final form of the shape equations from (15) and (17), we need the following relations

$$\begin{aligned}\frac{\partial\mathcal{L}}{\partial\psi} &= \frac{r}{4}\left(\dot{\psi} + \frac{\sin\psi}{r}\right)\frac{\cos\psi}{r} - M\frac{3r^2\cos\psi}{4} - N\frac{cos\psi}{4} - F\cos\psi + \Gamma\sin\psi \\ \frac{\partial\mathcal{L}}{\partial\dot{\psi}} &= \frac{r}{4}\left(\dot{\psi} + \frac{\sin\psi}{r}\right) - \frac{Nr}{4} \\ \frac{d}{ds}\left(\frac{\partial\mathcal{L}}{\partial\dot{\psi}}\right) &= \frac{\dot{r}}{4}\left(\dot{\psi} + \frac{\sin\psi}{r}\right) + \frac{r}{4}\left(\ddot{\psi} + \frac{\cos\psi\dot{\psi}}{r} - \frac{\sin\psi}{r^2}\dot{r}\right) - \frac{N\dot{r}}{4} \\ \frac{\partial\mathcal{L}}{\partial r} &= \frac{1}{8}\left(\dot{\psi} + \frac{\sin\psi}{r}\right)^2 - \frac{1}{4}\left(\dot{\psi} + \frac{\sin\psi}{r}\right)\frac{\sin\psi}{r} - M\frac{3r\cos\psi}{2} - \frac{L}{2} - N\frac{\dot{\psi}}{4} \\ \frac{\partial\mathcal{L}}{\partial\dot{r}} &= \Gamma \\ \frac{d}{ds}\left(\frac{\partial\mathcal{L}}{\partial\dot{r}}\right) &= \dot{\Gamma}.\end{aligned} \tag{18}$$

Using above relations, the Hamiltonian becomes

$$H = \frac{r}{8}\left(\dot{\psi}^2 - \frac{\sin^2\psi}{r^2}\right) + \frac{3Mr^2\sin\psi}{4} + \frac{Lr}{2} + \frac{N\sin\psi}{4} + \Gamma\cos\psi + F\sin\psi = 0 \tag{19}$$

and shape equations (15) simplifies to

$$\begin{aligned}\ddot{\psi}r &= \frac{\dot{r}\sin\psi}{r} - \dot{\psi}\dot{r} - 3Mr^2\cos\psi - 4F\cos\psi + 4\Gamma\sin\psi \\ \dot{\Gamma} &= \frac{1}{8}\left(\dot{\psi}^2 - \frac{\sin^2\psi}{r^2}\right) - \frac{3Mr\sin\psi}{2} - \frac{L}{2} - \frac{N\dot{\psi}}{4}.\end{aligned} \tag{20}$$

By substituting Γ from $(20)_1$ in (19) , we can write the final form of the shape equations. Finally eliminating s from the above equations, we can write the shape equations in terms of parameter r. The procedure is explained in detail in Project 2 [2]. I will skip the steps and directly use the important results. From equation 29 of Project 2, we have

$$\dot{\psi} = \cos\psi\psi', \qquad \ddot{\psi} = \cos\psi\left[-\sin\psi\psi'^2 + \cos\psi\psi''\right]. \tag{21}$$

Upon using the above equations, the final shape equation becomes

$$\begin{aligned}\psi''\cos\psi - \psi'^2\sin\psi = \frac{r}{2\cos^2\psi}\left[\frac{\sin\psi}{r}\left(\frac{\sin^2\psi}{r^2} - \psi'^2\cos^2\psi\right) - 6M - 4L\frac{\sin\psi}{r} - 2N\frac{\sin^2\psi}{r^2} - 8F\frac{1}{r^2}\right] \\ - \left(\frac{\psi'\cos\psi}{r} - \frac{\sin\psi}{r^2}\right),\end{aligned} \tag{22}$$

where the (') denotes the derivative w.r.t r.

3 Near pole contour angle

At the pole, $r \to 0$ and the equation (22) can be expanded in terms of r. Multiplying (22) by r^2,we get

$$\begin{aligned}r^2\psi''\cos\psi - r^2\psi'^2\sin\psi - \frac{\sin^3\psi}{2\cos^2\psi} + \frac{\sin\psi}{2}r^2\psi'^2 + 3Mr^3 + 2Lr^2\frac{\sin\psi}{\cos^2\psi} + Nr\frac{\sin^2\psi}{\cos^2\psi} + 4Fr\frac{1}{\cos^2\psi} \\ + r\psi'\cos\psi - \sin\psi = 0\end{aligned} \tag{23}$$

At the leading order the equation reduces to

$$\begin{aligned}\frac{\sin^3\psi}{2\cos^2\psi} + \sin\psi &= \mathcal{O}(r) \\ \sin\psi\left(1 + \frac{\sin^2\psi}{2\cos^2\psi}\right) = \mathcal{O}(r) &\implies \sin\psi = \mathcal{O}(r) \implies \psi = \mathcal{O}(r)\end{aligned}$$

Since $\psi \to 0$ as $r \to 0$, we can expand (23) in terms of ψ also. Dividing (23) by r and expanding in terms of ψ, we obtain

$$\begin{aligned}r\psi'' - r^2\psi'^2c_p + \frac{c_P}{2}r^2\psi'^2 + 3Mr + 2Lr^2c_p + Nr^2c_p^2 + 4F + \psi' - c_p = \mathcal{O}(\psi^2) \\ r\psi'' + 4F + \psi' - c_p = \mathcal{O}(\psi^2, r^2),\end{aligned}$$

where $c_p = \sin\psi/r \approx \psi/r$ is a principal curvature. Multiplying the above equation by r, we obtain a non-homogeneous Euler-Bernoulli equation at the leading order

$$r^2\psi'' + r\psi' - \psi = -4Fr.$$

The homogeneous solution is given by x^m, which upon substitution in the above equation gives $m = \pm 1$. Since we know that the ψ is of order $\mathcal{O}(r)$, we discard $m = -1$ solution. Then the homogeneous solution becomes $\psi_h = Br$, where B is a constant. For finding the non-homogeneous solution, we first substitute $r = e^t$ which transforms the above equation to a constant coefficient equation

$$\frac{d^2\psi}{dt^2} - \psi = Fe^t. \tag{24}$$

The homogeneous part of the equation has solutions $\psi = e^t, e^{-t}$. Therefore, we guess the non-homogeneous solution of the form $\psi = Kt \exp t$. Substituting the guess in the above equation we get $K = -2F$. Therefore the particular solution becomes $\psi_p = -2Fte^t = -2Fr \ln r$. hence, the final form of the solution becomes

$$\psi = \psi_h + \psi_p = (-2F \ln r + B)r. \tag{25}$$

This contour angle ψ at pole can now be used as an initial condition for solving the shape equation (22). The parameters M, L, N, F and B are chosen according to the given values v, a, Δa_0 and z_0 and to fulfill the condition that the transverse shear force Γ at the equator equals zero due to mirror symmetry.

4 Limiting Shapes

We can find the maximal length (z_0) of a vesicle with given volume (v), area ($a = 1$) and the area difference (Δa) by considering the dimensionless functional

$$\tilde{g} = z_0 - \tilde{M}v - \tilde{L}a - \tilde{N}\Delta a, \tag{26}$$

where $\tilde{M}$, $\tilde{L}$ and $\tilde{N}$ are Lagrange multipliers. At equilibrium,

$$\begin{aligned} \frac{\partial \tilde{g}}{\partial v} = 0 &\implies \tilde{M} = \frac{dz_0}{dv}, \\ \frac{\partial \tilde{g}}{\partial a} = 0 &\implies \tilde{L} = \frac{dz_0}{da}, \\ \frac{\partial \tilde{g}}{\partial \Delta a} = 0 &\implies \tilde{N} = \frac{dz_0}{d\Delta a}. \end{aligned} \tag{27}$$

Using the Fig. 1, we can express $\tilde{g}$ as

$$\tilde{g} = \int_{s_0}^{s_1} \tilde{L} ds,$$

where $\tilde{L}$ is the Lagrangian. Doing calculations similar to that shown in equation (12), we arrive at the result

$$\tilde{\mathcal{L}} = \sin\psi - \tilde{M}\frac{3r^2 \sin\psi}{4} - \tilde{L}\frac{r}{2} - \tilde{N}\frac{\sin\psi + \dot{\psi}r}{4} + \tilde{\Gamma}(\dot{r} - \cos\psi), \tag{28}$$

where the last term is due to the relation $(9)_1$. Making the first variation go to zero, we will arrive at the equations (15) and boundary conditions (16) where $\mathcal{L}$ is replaced by $\tilde{\mathcal{L}}$. Using the following results

$$\begin{aligned} &\frac{\partial \tilde{\mathcal{L}}}{\partial \psi} = \cos\psi - \tilde{M}\frac{3r^2 \cos\psi}{4} - \tilde{N}\frac{cos\psi}{4} + \tilde{\Gamma}\sin\psi \\ &\frac{\partial \tilde{\mathcal{L}}}{\partial \dot{\psi}} = -\frac{\tilde{N}r}{4}, \qquad \frac{d}{ds}\left(\frac{\partial \tilde{\mathcal{L}}}{\partial \dot{\psi}}\right) = -\frac{\tilde{N}\dot{r}}{4} \\ &\frac{\partial \tilde{\mathcal{L}}}{\partial r} = -\tilde{M}\frac{3r\cos\psi}{2} - \frac{\tilde{L}}{2} - \tilde{N}\frac{\dot{\psi}}{4} \\ &\frac{\partial \tilde{\mathcal{L}}}{\partial \dot{r}} = \tilde{\Gamma}, \qquad \frac{d}{ds}\left(\frac{\partial \tilde{\mathcal{L}}}{\partial \dot{r}}\right) = \dot{\tilde{\Gamma}}. \end{aligned} \tag{29}$$

in equations (15) (where $\mathcal{L}$ is replaced by $\tilde{\mathcal{L}}$), we arrive at the following Euler-lagrange equations

$$\cos\psi - \frac{3}{4}\tilde{M}r^2\cos\psi + \tilde{\Gamma}\sin\psi = 0,$$
$$\dot{\tilde{\Gamma}} + \frac{3\tilde{M}r\sin\psi}{2} + \frac{\tilde{L}}{2} + \frac{\tilde{N}\dot{\psi}}{4} = 0 \tag{30}$$

and Hamiltonian becomes

$$\tilde{H} = -\sin\psi + \frac{3\tilde{M}r^2\sin\psi}{4} + \frac{\tilde{L}r}{2} + \frac{\tilde{N}\sin\psi}{4} + \tilde{\Gamma}\cos\psi = 0. \tag{31}$$

Finally, eliminating $\tilde{\Gamma}$, as done in the last section, we arrive at the equation for the limiting shape

$$3\tilde{M}r^2 + 2\tilde{L}r\sin\psi + \tilde{N}\sin^2\psi - 4 = 0. \tag{32}$$

These limiting shapes are achieved at infinitely large axial forces. At the poles $r = 0$, we obtain

$$\sin^2\psi = \frac{4}{\tilde{N}}.$$

Therefore, the contour angles at both the poles are same and $\tilde{N} > 4$ for any solution to exist. Also since $\psi \neq 0$ at the pole, the vesicles are not smooth at the pole. The slopes on the two sides of the poles are given by

$$\psi = \pm\sin^{-1}\left(\sqrt{\frac{4}{\tilde{N}}}\right).$$

Also, from $(27)_1$, we find that $\tilde{\Gamma} = 0$ at the equator ($\psi = \pi/2$).

5 Prolate shapes with equatorial symmetry

We can obtain the equilibrium shapes of the vesicles by either directly using equation (22) or by using the set of equations (19), (20) and $(9)_1$. Equation (22) contains singularity at $\psi = \pi/2$ due to the presence of $\cos(\psi)$ in the denominator. Using *ode45* or *ode15s* in MatLab fails to solve for all r. The solution stops at the point where $\psi = \pi/2$. Therefore, we will use the set of equations (19), (20) and $(9)_1$ which contains singularity only at $r = 0$. The initial condition can be obtained from (25) and (19) as

$$\begin{aligned}
\psi_0 &= (-2F\ln(r_0) + B)r_0 \\
\dot{\psi}_0 &= (-2F\ln(r_0) + B) - 2F \\
\Gamma_0 &= \frac{-1}{\cos\psi_0}\left(\frac{r}{8}\left(\dot{\psi}_0^2 - \frac{\sin^2\psi_0}{r_0^2}\right) + \frac{3Mr_0^2\sin\psi_0}{4} + \frac{Lr_0}{2} + \frac{N\sin\psi_0}{4} + F\sin\psi_0\right) \\
r_0 &= s_0\cos\psi_0
\end{aligned} \tag{33}$$

where s_0, r_0, ψ_0, $\dot{\psi}_0$ and Γ_0 are initial values of s, r, ψ, $\dot{\psi}$ and Γ. The final arc length s_f is not known and hence we iterate for different values of s_f such that the relative area a equals one.

To validate the code, it should be tested against the simplest cases. The simplest cases include the case where $N = 0$ and $F = 0$. This corresponds to the case when there is no non-local bending modulus and no axial force. This case has been studied extensively in literature. To generate the shape we also need parameters L, M and B. One such set of parameters is available in Table I of [1] for the relative volume $v = 0.95$. Also the values of pole to pole distance z_0 and the radius at the equator r_e is provided. We can check our results with the z_0 and r_e output of our code. The final shape is shown in Fig. 2b. Also the parameters of the vesicle is given in Table 1. The shape from [1] is shown in Fig. 2a. We can see that both the shapes are same. The pole to pole distance $z_0 = 2.593$ and equatorial radius $r_e = 0.829$ matches exactly with that given in Table I of [1].

The second check is done for the case when there is no axial force but non-local bending modulus (N) is present. A sample parameters for this case is also present in Table I of [1] for $v = 0.95$. The shape found from our code doesn't form a closed shape as shown in Fig. 3. Also the volume $v = 1.0742$ shows that there is some inconsistency in the parameters we are using. Also, the shape is not symmetric about the equator. The shape reported in the [1] is shown in Fig. 4a. However, if we solve only till the equator, i.e. we stop the iteration when $a = 0.5$ and take mirror image about the equator for reconstructing the full picture then we get exactly the shape shown in Fig. 4a. The final shape is shown in Fig. 4b. The values $z_0 = 2.902$ and $r_e = 0.975$ from our result are closely matching with the values $z_0 = 2.901$ and $r_e = 0.973$ from [1].

From the shape shown in Fig. 3 it is clear that there doesn't exist equatorial mirror symmetry in the shape equation even when we imposed $\Gamma = 0$ at the equator. The symmetry has to be artificially imposed in the problem. However, in the absence of non-local bending modulus N, we saw from Fig. 2b that the equatorial symmetry exists.

Interestingly, we tried a second case with $N \neq 0$ and $F = 0$. The parameters are shown in Table 1 and are again borrowed from [1]. The shape obtained by us is shown in Fig. 5 and the shape from [1] is shown in Fig. 6a. In our case, we find an interesting heart like shape at the equator. The values $z_0 = 2.032$ and $r_e = 0.893$ varies significantly from the values $z_0 = 2.507$ and $r_e = 0.981$ given in [1]. Also, the relative volume $v = 0.63$ instead of $v = 0.95$ for which these parameters were given in the [1]. This is a significant mismatch. To attain the shape similar to Fig. 6a, we change our initial conditions. Originally, the initial condition is obtained from (33). Equations $(33)_1$ and $(33)_4$ are solved first using Newton-Raphson's method for r_0 and ψ_0. These values are substituted in $(33)_2$ and $(33)_3$ for $\dot{\psi}_0$ and Γ_0, respectively. In $(33)_4$, we assume some small value of s_0 because taking $s_0 = 0$ gives $r_0 = 0$ which leads to singularity in $(33)_1$. However, we will now discard equation $(33)_4$ and guess a value of r_0. Substituting this guessed values of r_0 in first three equations of (33), we will obtain the initial conditions. We will now implement the shooting method by changing r_0 such that v becomes 0.5. The increment in r_0 is done as follows

$$\delta v = g * (v - 0.5), \tag{34}$$

where g is the learning rate such that the required speed of convergence and accuracy is achieved. Increase g will increase the convergence speed but decrease the convergence radius. Therefore, for higher accuracy we require smaller g. The result with the shooting method is shown in Fig. 6b. We find that the shape now matches quite closely with that given in [1]. For Fig. 6b, $z_0 = 2.5157$ and $r_e = 0.962$ are quite close to that given in [1].

Finally, we tried to solve for the case when there is presence of axial force using the parameters given in [1]. Following the similar procedure of shooting method, we were able to obtain a shape shown in Fig. 7b with $z_0 = 3.382$ and $r_e = 0.927$ which matches with values $z_0 = 3.387$ and 0.926 of Fig. 7a reported in [1]. However, in this case we found that the shape is much more sensitive to the initial conditions. The value of initial radius for which we obtained this shape is $r_0 = 1.74812023e - 7$ because of this the convergence rate of the code is very slow. Figure. 8 shows the shape of vesicle for $r_0 = 1.74812083e - 7$. We can see that even a change in eighth significant digit can change the shape significantly.

6 Generating the parameters

Parameters L, M, N and B are reported in [1] for $v = 0.9$ and some given values of Δa and z_0. However, regenerating shapes using these parameters requires time consuming shooting method for guessing initial condition. Therefore, we tried to estimate our own parameters for a given value of z_0 and Δa. To find the parameters we used the gradient descent method. For a given function $f(\boldsymbol{x})$, the $\boldsymbol{x}$ is updated as

$$\boldsymbol{x}^{n+1} = \boldsymbol{x}^n - \boldsymbol{G}\nabla f(\boldsymbol{x}^n). \tag{35}$$

where n is the number of iteration $\boldsymbol{G}$ is the diagonal matrix that contains the learning rate of each parameter. By iterating sufficient number of times, the method will give a $\boldsymbol{x}_0$ such that $f(\boldsymbol{x}_0) = 0$. The function $f(\boldsymbol{x})$ is called the loss function. We assumed the loss function as

$$f(\boldsymbol{x}) = w_1\big|v_n - V\big| + w_2\big|a_n - A\big| + w_3\big|\Delta a_n - \Delta A\big| + w_4\big|z_n - Z\big|, \tag{36}$$

where v_n is the volume, a_n is the area, Δa_n is the area difference and z_n is the distance between the poles. The subscript n represents the values at n^{th} iteration. V is the desired volume, A is the desired area, Z is the desired pole distance and ΔA is the desired area difference. w_1, w_2, w_3 and w_4 are weight functions. Weight functions can be adjusted to optimize our results. For example, increasing w_1 will give volume closer to V. Another tuning parameter is the learning rate. For parameters that vary significantly the learning rates should be small otherwise the required accuracy will not be achieved. The parameters for which we solve are

$$\boldsymbol{x} = \begin{bmatrix} M \\ L \\ N \\ B \\ F \\ s \end{bmatrix}, \tag{37}$$

where s is the arc length of the axi-symmetric curve. The gradient of $f(\boldsymbol{x})$ is found by approximating the partial differentiation as follows

$$\frac{\partial f}{\partial M} = \frac{f(M + \delta M, L, F, N, B, s) - f(M - \delta M, L, F, N, B, s)}{2\delta M}. \tag{38}$$

To find gradient for any given value of M, the equations (33) is solved for both parameters $M + \delta M$ and $M - \delta M$. Then the change in loss function is computed. δM is again a parameter to adjust the accuracy. This procedure is repeated for all parameters. In the start of the iteration we guess initial values of the parameters and then it is allowed to evolve until value of loss function goes below a minimum value i.e. $1e - 3$.

The convergence of this gradient descent method is again a challenging task. There are two ways to speed up the convergence. First method is dynamic learning rates such that it is big when error is more but small at smaller errors. We implement this by reducing the learning rates by 1/2 when error becomes 1/2 of the original. Second method is by adjusting weight functions. We usually keep big values for w_1 and w_2 such that the required area and the volume of the vesicle is attained. The deviation in pole height and area difference doesn't matter a lot since the vesicle shape obtained is valid. Also, now we don't require shooting method for initial condition. As, we are not assuming any symmetry at the equator, we can also generate shapes without equatorial symmetry.

To check the results of the gradient descent method, we first generated the shapes for reduced volume $v = 0.95$ when $F = 0$ and $N = 0$. Figure 9 shows the shape when $w_3 = w_4 = 0$. The values $z_0 = 2.501$ and $\Delta_a = 0.513$ are close to that reported in [1]. Only significant difference is in the value of parameter B. For our case $B = 1.423$ while [1] reports $B = 1.490$. Therefore, without guessing the initial condition, we are able to generate the shape using parameters obtained by gradient descent method. Since we now have our on parameters we can generate shape with different v. For $v = 0.99$, we have nearly circular shape with $z_0 = 1.999$ and $r_e = 0.98$. The shape is shown in 10. Figure 11 shows the shape when $v = 0.5$ and Fig. 12 shows the shape when $v = 0.3$. We can see that the equator is elongated.

Changing parameters also changes the results significantly. Changing the value of M from -1.882 to -3.882 changes the shape as shown in Fig. 13. We find that the radius at the equator is reduced to 0.2778. Figure 14 shows the shape when L is changed from 2.682 to 6.682. The equator is further stretched and $r_e = 1.349$.

Figure 15 and 16 shows the shape when $N \neq 0$. There is stretching at the poles even in the absence of axial force. Figure 17 represents the shape when $v = 0.7$. The equator starts to shrink as v increases.

Finally, we generate parameters when $F \neq 0$. When $F \neq 0$, the convergence is very slow. So, we initialize it very close to the parameters given in [1]. The shape obtained is shown in 18. The convergence is fast when we reduce the value of v. Figure 19 shows the shape when $v = 0.7$. The shape has sharp edges at the equator.

7 Shapes with no mirror symmetry

We tried to find the shapes without assuming mirror symmetry about the equator. Initially, we assumed $N = 0$ and $F = 0$. For$v = 0.95$ and the parameters used for Fig. 2b. We arrived at the shape similar to Fig. 2b . For $v = 0.9$ and $v = 0.7$ the shapes were not closed as shown in Fig. 20 and 21. . To find the closed shape we modified our loss function as follows

$$f(\boldsymbol{x}) = w_1\big|v_n - V\big| + w_2\big|a_n - A\big| + w_3\big|\Delta a_n - \Delta A\big| + w_4\big|z_n - Z\big| + \big|r_0\big|, \tag{39}$$

where r_0 is the radius at the other end of the pole. Using this form of loss function for $v = 0.95$ changed the shape of vesicle from Fig. 2b to 22. For $v = 0.79$,we obtained the shape shown in Fig. 23. We can see that the shape is not symmetric about the equator.

8 Limiting shapes

Equation (32) gives the limiting shapes of the vesicles. The equation is quadratic in $\sin\psi$. Solving the quadratic equation gives

$$\sin\psi = \frac{-2\tilde{L}r \pm \sqrt{(2\tilde{L}r)^2 - 4\tilde{N}(3\tilde{M}r^2 - 4)}}{2\tilde{N}} \tag{40}$$

The limiting shape of the vesicle for $\tilde{L} = 8.444$, $\tilde{M} = -6.486$ and $\tilde{N} = 4.463$ is shown in Fig. 24. For $\tilde{N} = 4$, the angle at pole becomes $\pi/2$. Figure 25 shows the limiting shape when $\psi_0 = \pi/2$.

9 Conclusion

We have derived the Euler-Lagrange equation for deriving the shape equations when axial force and non-local bending modulus is present. We obtained shapes for different parameters given in [1] using shooting method. We also obtained our own parameters using gradient descent method and showed that the shape may have no mirror symmetry about the equator. Convergence of the gradient descent method is bad for the cases when axial force F is present. Finally, we obtained the limiting shapes for the vesicles.

References

[1] Bojan Bozic, Sasa Svetina, and Bostjan Zeks. Theoretical analysis of the formation of membrane microtubes on axially strained vesicles. *Phys. Rev. E*, 55:5834–5842, May 1997.

[2] Kumar Gaurav. Shape equations of the axisymmetric vesicles.

[3] Hu Jian-Guo and Ou-Yang Zhong-Can. Shape equations of the axisymmetric vesicles. *Phys. Rev. E*, 47:461–467, Jan 1993.

Figures

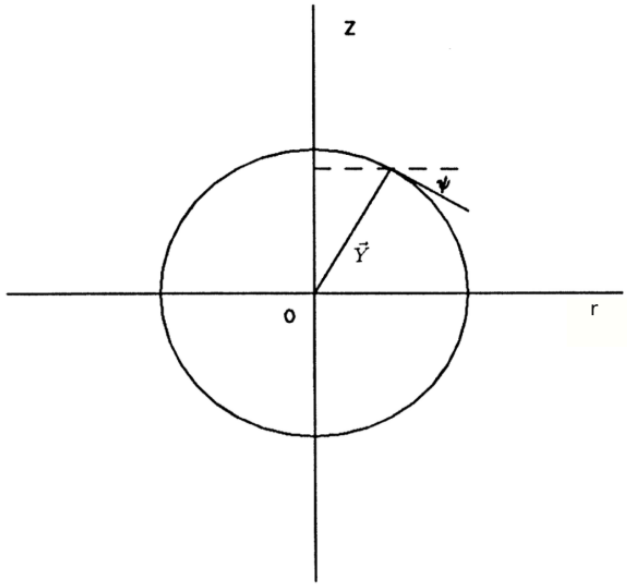

Figure 1: Schematic diagram of axisymmetric vesicle . Source: [3]

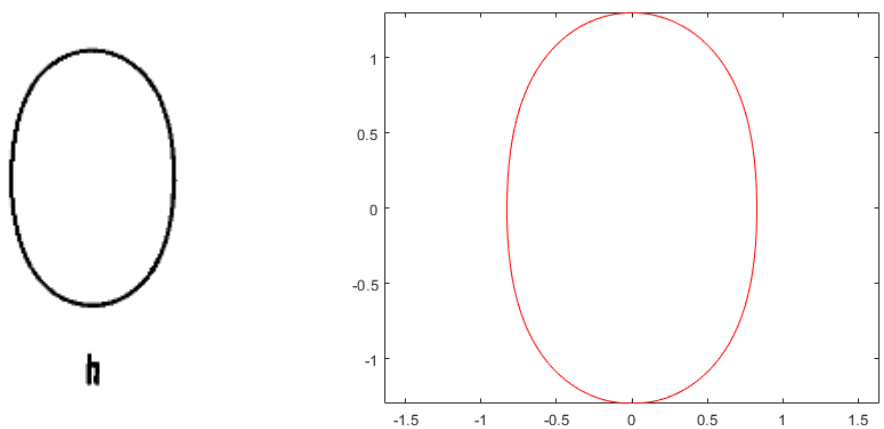

(a) (b)

Figure 2: Vesicle shape when there is no non-local bending effects and no axial force. (a) shape from our code (b) shape as reported in [1]

.

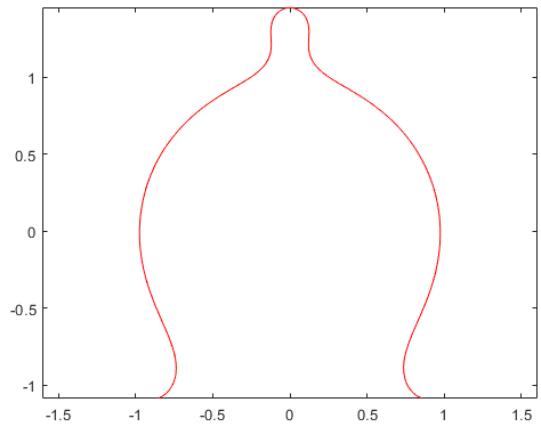

Figure 3: Vesicle shape when there is non-local bending effect present but in the absence of axial force

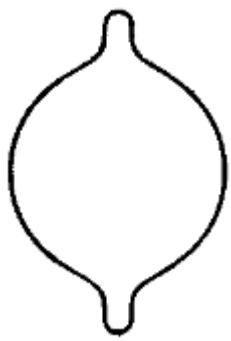

(a)

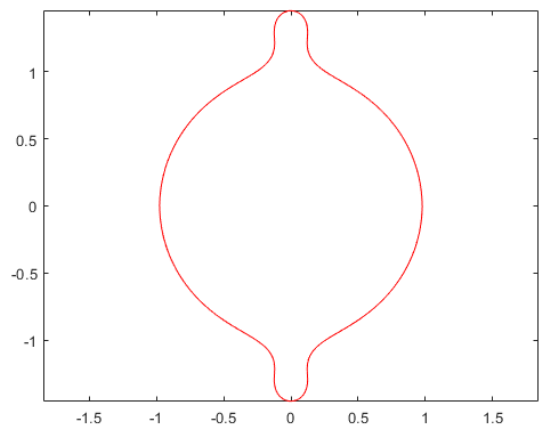

(b)

Figure 4: Vesicle shape when there is non-local bending effects present but in the absence of axial force. (a) shape as reported in [1] (b)shape from our code.

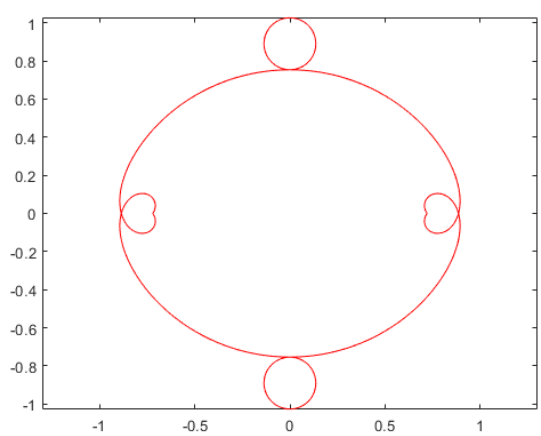

Figure 5: Vesicle shape when there is non-local bending effect and but no axial force

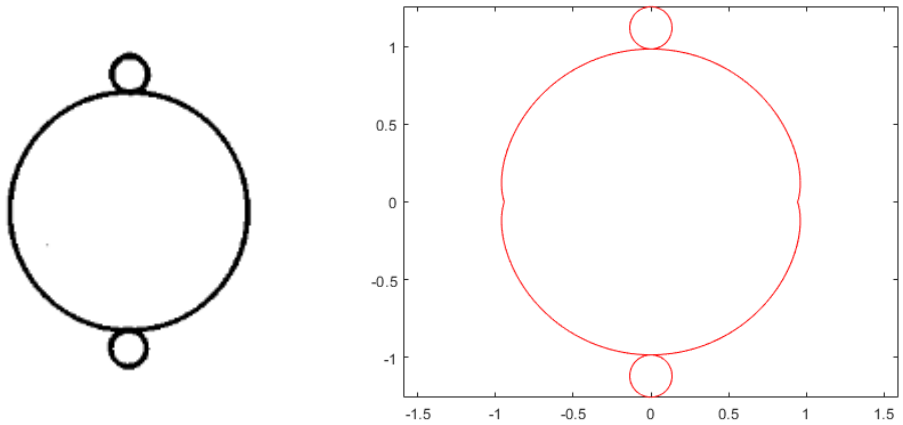

(a) (b)

Figure 6: Vesicle shape when there is non-local bending effects present but in the absence of axial force. (a) shape as reported in [1] (b) shape from our code.

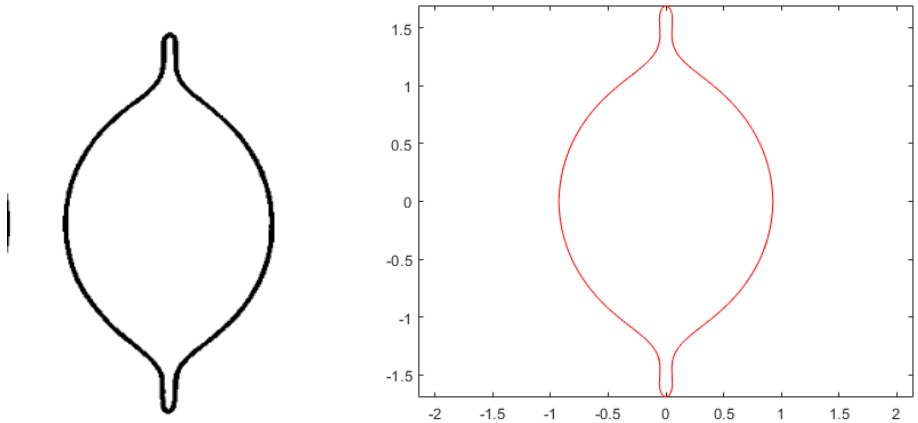

(a) (b)

Figure 7: Vesicle shape when there is both non-local bending effects and axial force present. (a) shape as reported in [1] (b) shape from our code

.

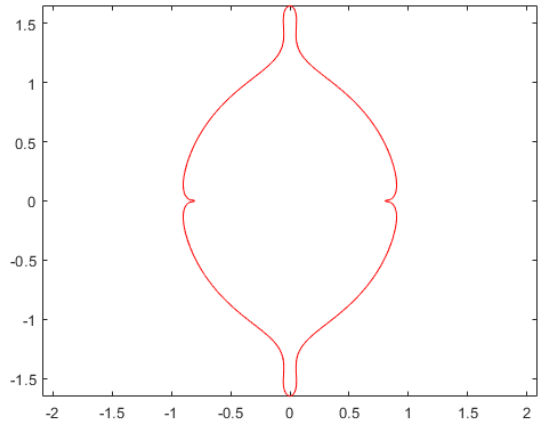

Figure 8: Vesicle shape when there is both non-local bending effects and axial force present but initial condition is changed slightly.

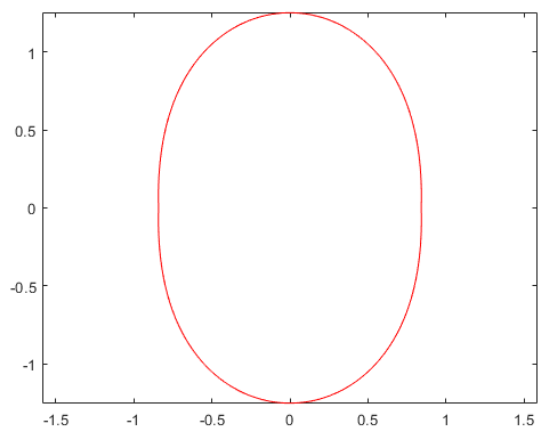

Figure 9: Vesicle shapes generated with new parameters when $N = 0$ and $F = 0$ ($v = 0.95$).

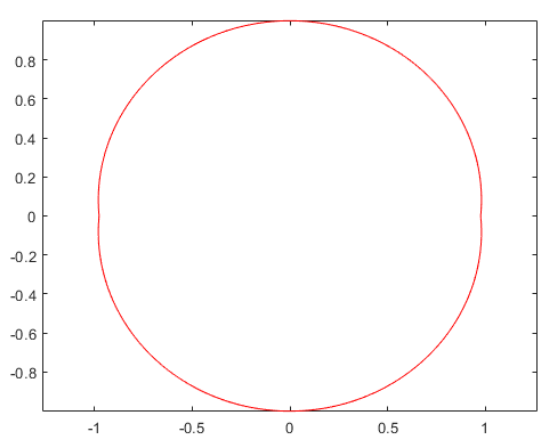

Figure 10: Vesicle shapes generated with new parameters when $N = 0$ and $F = 0$ ($v = 0.99$).

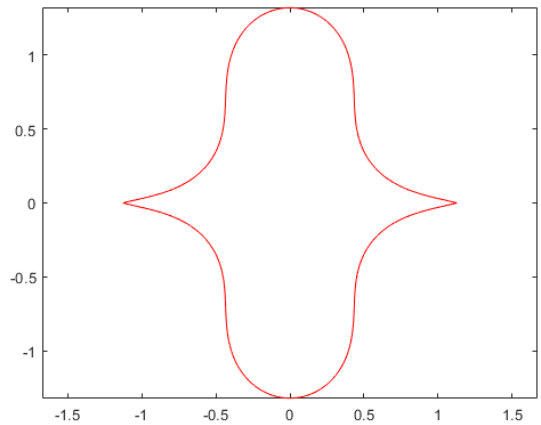

Figure 11: Vesicle shapes generated with new parameters when $N = 0$ and $F = 0$ ($v = 0.50$).

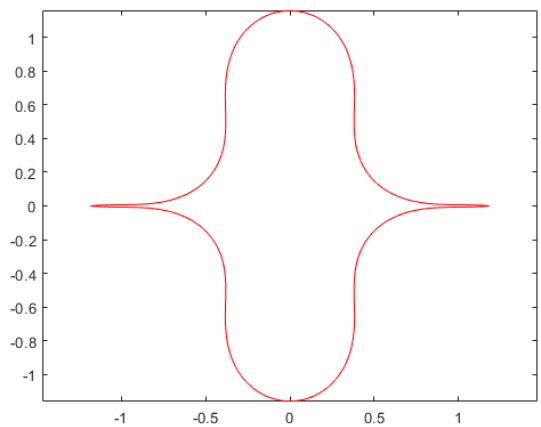

Figure 12: Vesicle shapes generated with new parameters when $N = 0$ and $F = 0$ ($v = 0.30$).

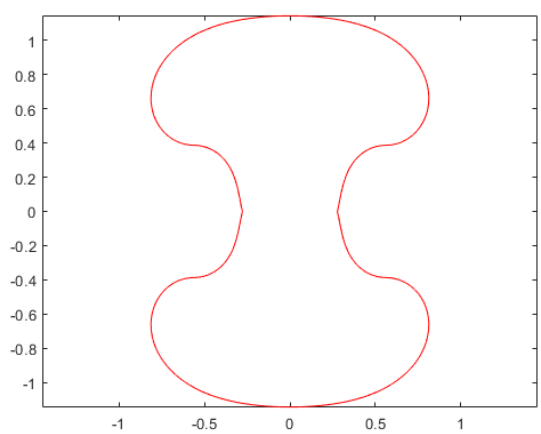

Figure 13: Vesicle shapes generated with new parameters when $N = 0$ and $F = 0$ ($M = -1.882$).

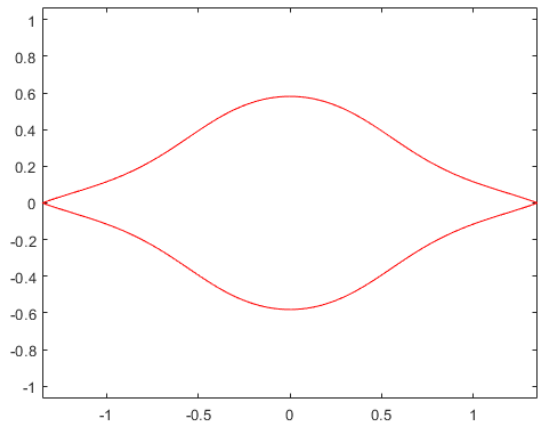

Figure 14: Vesicle shapes generated with new parameters when $N = 0$ and $F = 0$ ($L = 6.682$).

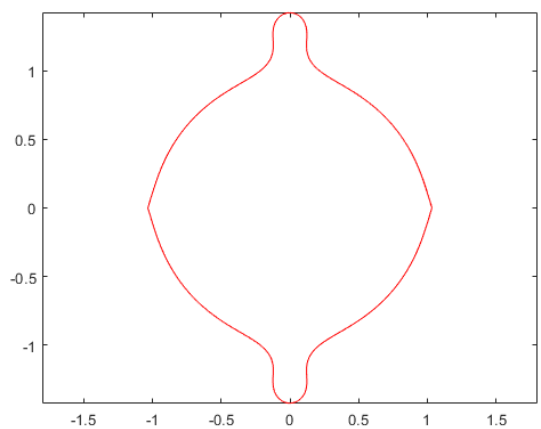

Figure 15: Vesicle shapes generated with new parameters when $N \neq 0$ and $F = 0$ ($N = 7.629$).

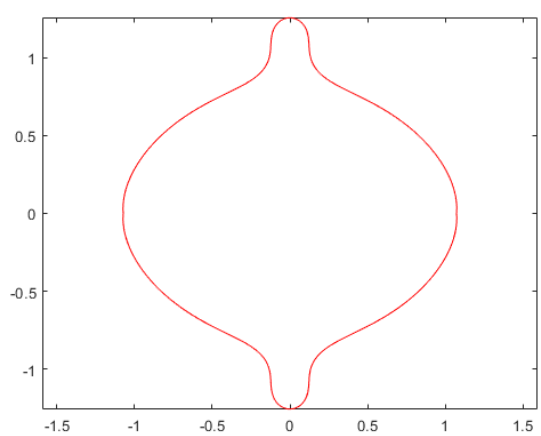

Figure 16: Vesicle shapes generated with new parameters when $N \neq 0$ and $F = 0$ ($N = 8.629$).

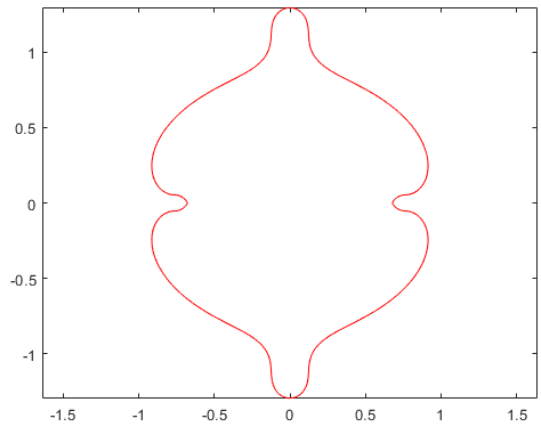

Figure 17: Vesicle shapes generated with new parameters when $N \neq 0$ and $F = 0$ ($v = 0.7$).

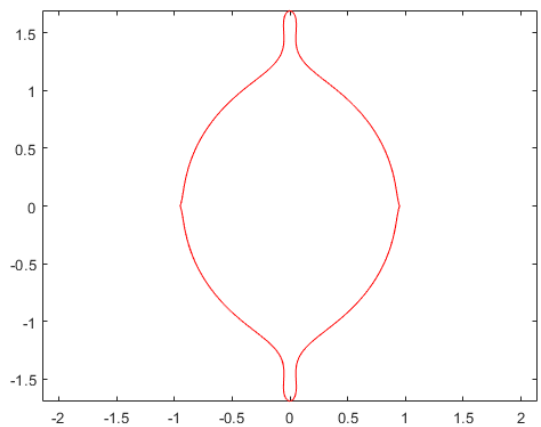

Figure 18: Vesicle shapes generated with new parameters when $N \neq 0$ and $F \neq 0$ ($v = 0.95$).

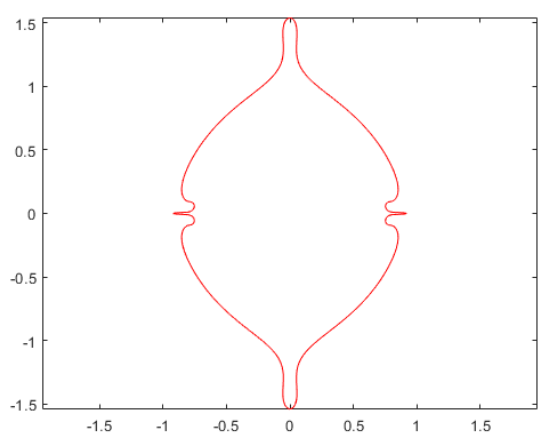

Figure 19: Vesicle shapes generated with new parameters when $N \neq 0$ and $F \neq 0$ ($v = 0.7$).

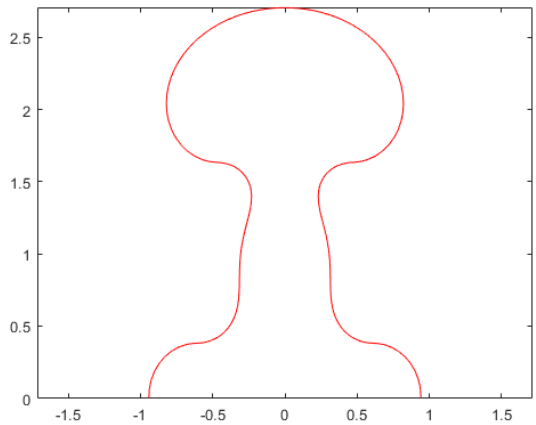

Figure 20: Vesicle shapes generated without equatorial symmetry when $N = 0$ and $F = 0$ ($v = 0.9$).

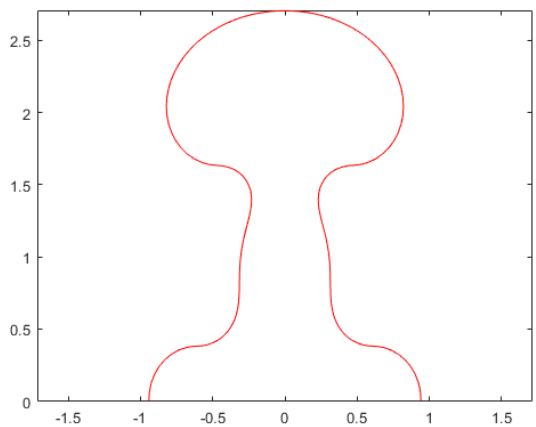

Figure 21: Vesicle shapes generated without equatorial symmetry when $N = 0$ and $F = 0$ ($v = 0.7$).

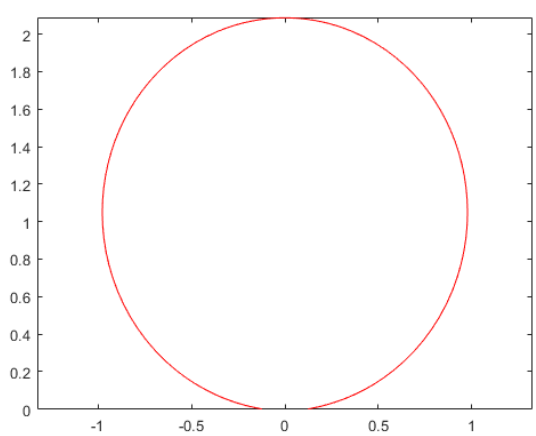

Figure 22: Vesicle shapes generated without equatorial symmetry when $N = 0$ and $F = 0$ ($v = 0.95$).

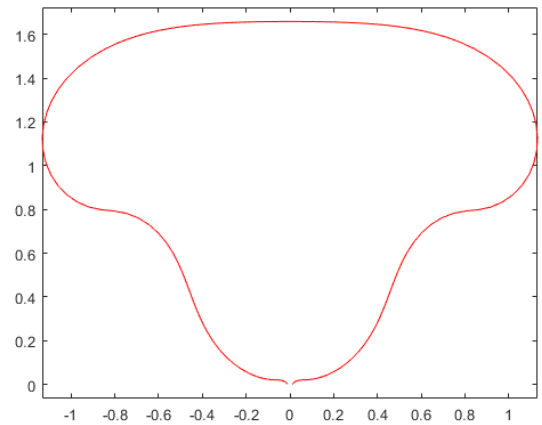

Figure 23: Vesicle shapes generated without equatorial symmetry when $N = 0$ and $F = 0$ ($v = 0.79$).

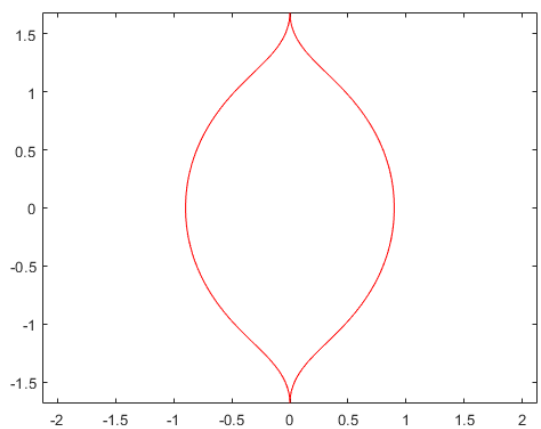

Figure 24: Limiting shapes for $N = 4.463$.

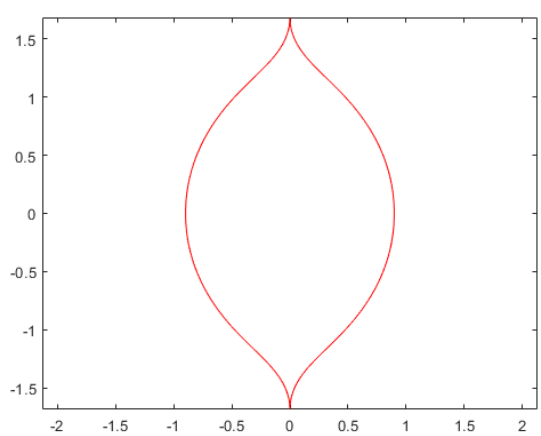

Figure 25: Limiting shapes for $N = 4.463$.

Tables

Figure	B	M	L	N	F
2	1.490	-1.882	2.682	0	0
3	9.078	9.558	-17.866	7.629	0
4	9.078	9.558	-17.866	7.629	0
5	7.348	20.7	-34.9	8.35	0
6	7.348	20.7	-34.9	8.35	0
7	-9.565	65.539	-101.497	-1.158	5.184
8	-9.565	65.539	-101.497	-1.158	5.184
9	1.423	-1.882	2.682	0	0
10	1.223	-1.882	2.682	0	0
11	2.423	-1.882	2.682	0	0
12	2.9133	-1.882	2.682	0	0
13	0.5157	-3.882	2.682	0	0
14	1.5868	-1.882	6.682	0	0
15	9.085	9.558	-17.866	7.629	0
16	9.615	7.558	-17.866	8.629	0
17	9.546	7.558	-17.866	8.629	0
18	-9.565	65.539	-101.497	-1.158	5.184
19	-9.565	65.539	-101.497	-1.158	5.184
20	1.490	-1.882	2.682	0	0
21	1.490	-1.882	2.682	0	0
23	0.1874	-1.882	1.597	0	